Nonadiabatic Time-Dependent Wave Packet Study of the $D^+ + H_2$ Reaction System

Tian-Shu Chu and Ke-Li Han*

State Key Laboratory of Molecular Reaction Dynamics, Dalian Institute of Chemical Physics, Chinese Academy of Sciences, Dalian 116023, China

Received: October 25, 2004; In Final Form: December 23, 2004

A theoretical investigation on the nonadiabatic processes of the $D^+ + H_2$ reaction system has been carried out by means of exact three-dimensional nonadiabatic time-dependent wave packet calculations with an extended split operator scheme (XSOS). The diabatic potential energy surface newly constructed by Kamisaka et al. (*J. Chem. Phys.* **2002**, *116*, 654) was employed in the calculations. This study provided quantum cross sections for three competing channels of the reactive charge transfer, the nonreactive charge transfer, and the reactive noncharge transfer, which contrasted markedly to many previous quantum theoretical reports on the $(DH_2)^+$ system restricted to the total angular momentum $J = 0$. These quantum theoretical cross sections derived from the ground rovibrational state of H_2 show wiggling structures and an increasing trend for both the reactive charge transfer and the nonreactive charge transfer but a decreasing trend for the reactive noncharge transfer throughout the investigated collision energy range 1.7−2.5 eV. The results also show that the channel of the reactive noncharge transfer with the largest cross section is the dominant one. A further investigation of the v-dependent behavior of the probabilities for the three channels revealed an interesting dominant trend for the reactive charge transfer and the nonreactive charge transfer at vibrational excitation $v = 4$ of H_2. In addition, the comparison between the centrifugal sudden (CS) and exact calculations showed the importance of the Coriolis coupling for the reactive system. The computed quantum cross sections are also compared with the experimental measurement results.

1. Introduction

From the theoretical point of view, interest in the $(H + H_2)^+$ system and its HD and D_2 variants[1−14] derives from its simplicity and its rich reaction dynamics. The highest level of theory can be applied to study the reaction system containing only three light atoms. In this reaction system, the charge transfer processes taking place on several potential energy surfaces have received more and more attention due to their highly significant importance in the nonadiabatic dynamics fields. Actually, some theoretical nonadiabatic studies of this system and its isotopic variants,[9−11] as well as many other studies on the reactions of $F + H_2 \rightarrow H + HF$,[15−18] $Cl + H_2 \rightarrow H + HCl$,[19,20] $O + H_2 \rightarrow H + OH$,[21,22] and so forth, have been carried out recently. Both trajectory surface hopping methods and quantum mechanical methods were employed in the efforts to elucidate the reaction mechanisms induced by the nonadiabatic transitions. Being a paradigm for reactions accompanied by nonadiabatic transitions, the $(H + H_2)^+$ system, along with its isotopically substituted system, lends itself to many accurate nonadiabatic quantum calculations. Such quantum studies have been carried out by Markovic et al.,[7] Last et al.,[8] Ushakov et al.,[9] Takayanagi et al.,[10] and Kamisaka et al.[11] By using Johnson's hyperspherical coordinates and the iterative Lanczos reduction propagation technique in a time-dependent wave packet study, Markovic et al.[7] presented their results on the $D^+ + H_2$ system for the total angular momentum $J = 0$, but they met with the problem of slow convergence due to the deep well on the ground surface. The calculated cross sections and the opacity functions for the charge transfer process in the $H + H_2^+$ reaction system were reported by Last et al.,[8] who carried out a time-independent calculation with coupled states approximation. Ushakov et al.[9] investigated the collinear $H^+ + H_2$ system within a time-independent framework and revealed a strong dependence of the nonadiabatic transition probability on the initial vibrational state of H_2. Ion−molecule collisions of D^+ with H_2 were studied by Takayanagi et al.,[10] using also the time-independent approach, but they only presented the cumulative reaction probability for $J = 0$. Recently, Kamisaka et al.[11] have reported on an extensive time-independent quantum study for the $(D + H_2)^+$ system and calculated the cumulative transition probabilities of $J = 0$ for six given adiabatic and nonadiabtic processes of the reaction systems. Up to now, however, these elaborating quantum calculations of the $(D + H_2)^+$ system were all limited to the total angular momentum $J = 0$, and no theoretical quantities comparable to experimental observables have been achieved in the investigated energy range. Furthermore, like the previously published studies on the $O + H_2$,[23,24] $H + O_2$,[25,26] and $C + H_2$[27,28] systems in which the deep well challenges the accurate quantum dynamics methods, the accurate nonadiabatic quantum calculation on the $(D + H_2)^+$ system is complicated by the presence of the rather deep singlet well of the system.

In this paper, we report for the first time on the exact quantum total reaction cross sections for three competing channels in the $D^+ + H_2$ reaction system for the ground rovibrational initial state of H_2 over collision energies of 1.7−2.5 eV. It is hoped that this will contribute to the understanding of the nonadiabatic properties in this system by carrying out several three-dimensional nonadiabatic wave packet studies, utilizing an extended split operator scheme (XSOS) developed for treating the multi-potential energy surface (PES) problem.[29,30] The idea of achieving a direct comparison between theoretical quantum calculations and experiments also stimulated the present work. In addition, the comparison between the coupled channel (CC)[31]

10.1021/jp0451391 CCC: $30.25
Published on Web 02/18/2005

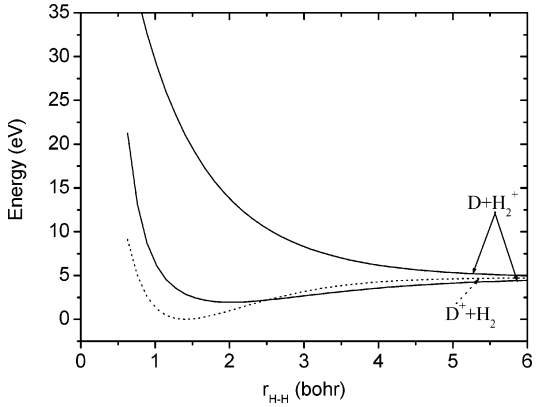

Figure 1. Cuts through the entrance channel in the asymptotic region ($R \rightarrow \infty$). The dotted curve depicts the ground potential energy surface $1^1A'$, while the solid curves represent the excited potential energy surfaces $2^1A'$ and $3^1A'$.

and centrifugal sudden (CS) approximation[32,33] calculations of the system will enable us to discuss the accuracy of the CS approximation to the reaction.

The three investigated channels are the reactive charge transfer (RCT), the nonreactive charge transfer (NRCT), and the reactive noncharge transfer (RNCT):

$$D^+ + H_2 \rightarrow DH^+ + H \qquad \text{RCT} \qquad (1.1)$$

$$D^+ + H_2 \rightarrow D + H_2^+ \qquad \text{NRCT} \qquad (1.2)$$

$$D^+ + H_2 \rightarrow H^+ + HD \qquad \text{RNCT} \qquad (1.3)$$

Nonadiabtic wave packet calculations on rather accurate and ab initio based potential energy surfaces are presented in order to obtain the reaction probabilities and cross sections over the collision energy range 1.7−2.5 eV as well as to quantify the role of H_2 vibrational excitation in the nonadibatic transitions.

In Figure 1, we depict the schematic energy profile of the $(DH_2)^+$ system in adiabatic representation. The electronic structure of the $(DH_2)^+$ system has the features of an adiabatic ground surface $1^1A'$ with a deep well and correlating asymptotically to the $D^+ + H_2$ reactant, while the first excited surface $2^1A'$, which is repulsive, correlates asymptotically to the $D + H_2^+$ reactant and the second excited surface $3^1A'$, which is also repulsive, is lying on a rather higher level. In the region far away from the geometry of the DH_2^+ triatomic complex, there are crossing seams of the two surfaces $1^1A'$ and $2^1A'$. At least these three potential energy surfaces should be taken into account in the dynamics of the $D^+ + H_2$ reaction, which can be described within a diabatic coupling representation by using the 3×3 diatomics-in-molecule (DIM) PES or the derived 3×3 PES from the DIM PES by adding some correction terms.

This paper is organized as follows. Section II describes the potential energy used for this study. The method of dynamics calculations is presented in section III. Then, section IV presents the calculated results and the discussion. The summary is in section V.

2. Potential Energy Surfaces

We use the same diabatic KBNN potential energy surface as that in ref 11, which was a newly developed surface consisting of a 3×3 DIM potential matrix and three-body correction terms. To improve the fitting accuracy in the total energy range 2.0−2.6 eV, 577 ab initio energy points for the ground state surface and 79 points for the first excited state surface were used to determine the fitting parameters of the KBNN surface. There was a deep well of ∼4.0 eV on the corresponding adiabatic ground surface of the KBNN, which was also characterized by a smaller long-range attractive force and by the vanished fake barrier around a hyperradius of 8 au,[11] as compared with the previously constructed DIM surface.[9] The contour maps of the adiabatic surfaces for the ground state and for the first exited state, along with the coupling between them, are shown in Figure 2. More details can be found in ref 11.

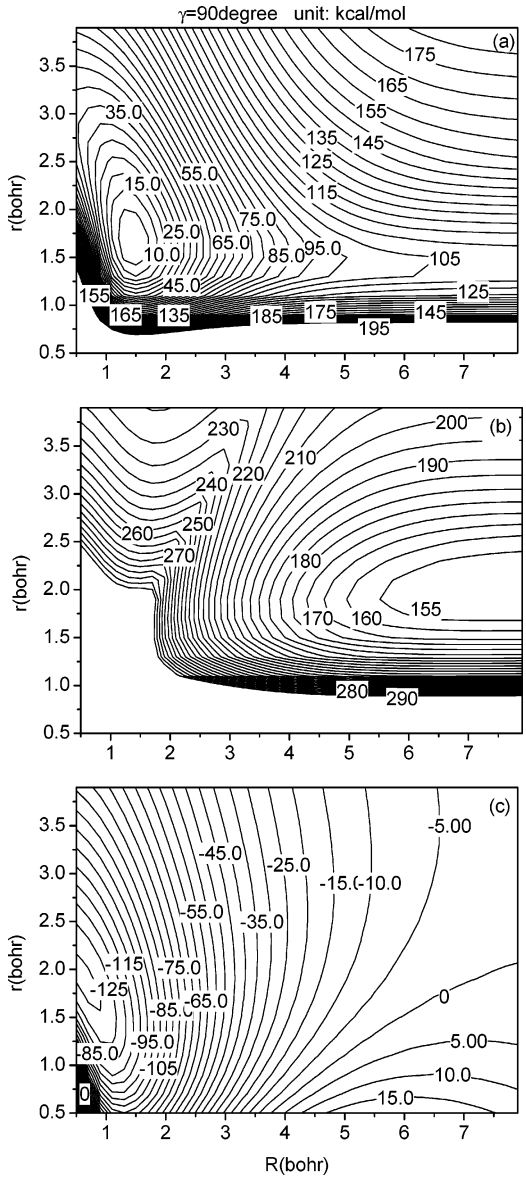

Figure 2. Contour plots of potential energy surfaces of the $D^+ + H_2$ system as a function of Jacobi coordinates (R, r, γ): (a) the adiabatic ground state; (b) the adiabatic first excited state; (c) coupling between the ground state and the first excited state.

3. Time-Dependent Wave Packet Calculations for Multi-Potential Surfaces

Since the descriptions of the time-dependent wave packet calculation using the split operator propagation method for the single-surface problem can be found in many published papers[34−38] and the details of the nonadiabatic quantum dynamics method are described in ref 29, here we only give a brief outline.

The time-dependent Schrodinger equation for a triatomic system involving more than one potential energy surface can be written in a diabatic representation as

$$i\hbar\frac{\partial}{\partial t}\begin{bmatrix}\psi_1\\ \psi_2\\ \psi_3\end{bmatrix} = H_0\begin{bmatrix}\psi_1\\ \psi_2\\ \psi_3\end{bmatrix} + V_{\text{rot}}\begin{bmatrix}\psi_1\\ \psi_2\\ \psi_3\end{bmatrix} + \begin{bmatrix}V_{11} & V_{12} & V_{13}\\ V_{21} & V_{22} & V_{23}\\ V_{31} & V_{32} & V_{33}\end{bmatrix}\begin{bmatrix}\psi_1\\ \psi_2\\ \psi_3\end{bmatrix} \tag{2.1}$$

where in terms of Jacobi coordinates

$$H_0 = -\frac{\hbar^2}{2\mu_R}\frac{\partial^2}{\partial R^2} + h(r) \tag{2.2}$$

$$h(r) = -\frac{\hbar^2}{2\mu_r}\frac{\partial^2}{\partial r^2} + V_r(r) \tag{2.3}$$

$$V_{\text{rot}} = \frac{(J-j)^2}{2\mu_R R^2} + \frac{j^2}{2\mu_r r^2} \tag{2.4}$$

the usual definitions of R, r, μ_R, μ_r, $V_r(r)$, J, and j can be found in ref 35. ψ_i ($i = 1$, 2, or 3) is the component of the total unitary wave function relating to each of the three potential energy surfaces. The wave function is expanded in terms of translational basis $U_n^v(R)$, vibrational basis $\phi_v(r)$, and the body-fixed (BF) total angular momentum eigenfunction $Y_{jK}^{JM\epsilon}(\hat{R}, \hat{r})$.[35]

In the exact treatment, the operation of the orbital angular momentum (or centrifugal potential) operator on the BF total angular momentum eigenfunction can be written as[39,40]

$$\frac{\hbar^2}{2\mu_R R^2}\langle Y_{jK}^{JM\epsilon}|(J-j)^2|Y_{j'K'}^{JM\epsilon}\rangle =$$

$$\frac{\hbar^2}{2\mu_R R^2}\delta_{j,j'}\{[J(J+1)+j(j+1)-2K^2]\delta_{KK'} -$$

$$\lambda_{jK}^{+}\lambda_{jK}^{+}(1+\delta_{K0})^{1/2}\delta_{K+1,K'} - \lambda_{jK}^{-}\lambda_{jK}^{-}(1+\delta_{K1})^{1/2}\delta_{K-1,K'}\} \tag{2.5}$$

and λ is defined as

$$\lambda_{AB}^{\pm} = [A(A+1) - B(B\pm 1)]^{1/2} \tag{2.6}$$

As can be seen, the centrifugal potential in the BF representation is not diagonal. Different K channels are coupled through the centrifugal potential for the total angular momentum $J > 0$. In the centrifugal sudden approximation[32,33] for the total angular momentum $J > 0$, the off-diagonal terms in eq 2.5 are neglected to give the following CS result

$$\frac{\hbar^2}{2\mu_R R^2}\langle Y_{jK}^{JM\epsilon}|(J-j)^2|Y_{j'K'}^{JM\epsilon}\rangle = \frac{\hbar^2}{2\mu_R R^2}\delta_{j,j'}[J(J+1)+j(j+1)-2K^2]\delta_{KK'} \tag{2.7}$$

After the initial wave packet had been prepared, it was then propagated using the XSOS.[29,30] For a time step Δ, the propagation of the wave function can be treated as follows

$$\begin{bmatrix}\psi_1(t+\Delta)\\ \psi_2(t+\Delta)\\ \psi_3(t+\Delta)\end{bmatrix} =$$

$$e^{-iH_0\Delta/2}e^{-iV_{\text{rot}}\Delta/2}e^{-i\begin{bmatrix}V_{11} & V_{12} & V_{13}\\ V_{21} & V_{22} & V_{23}\\ V_{31} & V_{32} & V_{33}\end{bmatrix}\Delta}e^{-iV_{\text{rot}}\Delta/2}e^{-iH_0\Delta/2}\begin{bmatrix}\psi_1(t)\\ \psi_2(t)\\ \psi_3(t)\end{bmatrix}$$

$$= e^{-iH_0\Delta/2}e^{-iV_{\text{rot}}\Delta/2}Te^{-i\begin{bmatrix}V_1 & 0 & 0\\ 0 & V_2 & 0\\ 0 & 0 & V_3\end{bmatrix}\Delta}$$

$$\tilde{T}e^{-iV_{\text{rot}}\Delta/2}e^{-iH_0\Delta/2}\begin{bmatrix}\psi_1(t)\\ \psi_2(t)\\ \psi_3(t)\end{bmatrix}$$

$$= e^{-iH_0\Delta/2}e^{-iV_{\text{rot}}\Delta/2}T\begin{bmatrix}e^{-iV_1\Delta} & 0 & 0\\ 0 & e^{-iV_2\Delta} & 0\\ 0 & 0 & e^{-iV_3\Delta}\end{bmatrix}$$

$$\tilde{T}e^{-iV_{\text{rot}}\Delta/2}e^{-iH_0\Delta/2}\begin{bmatrix}\psi_1(t)\\ \psi_2(t)\\ \psi_3(t)\end{bmatrix} \tag{2.8}$$

where T is the unitary transform matrix, which is determined by diagonalizing the real potential matrix

$$\begin{bmatrix}V_{11} & V_{12} & V_{13}\\ V_{21} & V_{22} & V_{23}\\ V_{31} & V_{32} & V_{33}\end{bmatrix} \tag{2.9}$$

to

$$\begin{bmatrix}V_1 & 0 & 0\\ 0 & V_2 & 0\\ 0 & 0 & V_3\end{bmatrix} \tag{2.10}$$

$\tilde{T}$ is the transposed matrix of T.

The initial specified total reaction probabilities are finally obtained on the surfaces of relevance by calculating the reaction flux at a fixed surface $s = s_0$.[35]

$$P^J(E) = \sum_i \frac{\hbar}{\mu}\text{Im}\left[\left\langle \psi_i(E)\middle|\delta(s-s_0)\frac{\partial}{\partial s}\middle|\psi_i(E)\right\rangle\right] \tag{2.11}$$

For a reactive process, $s =$ r and $\mu = \mu_r$; for a nonreactive process, $s = R$ and $\mu = \mu_R$. The total reaction cross sections are calculated by

$$\sigma(E) = \frac{\pi}{k_0^2}\sum_J (2J+1)P^J(E) \tag{2.12}$$

with $k_0 = \sqrt{2\mu_R E}$ and E is the collision energy.

4. Results and Discussion

To get converged results, the following parameters were first determined by a preliminary test and then used in the calculations: 300 translational basis functions for the R coordinate in the range $0.2-22a_0$, 140 vibrational basis functions for the r coordinate from $0.5a_0$ to $15.0a_0$, $j_{\max} = 100$ for rotational basis, and a total propagation time of 30 000 au. Both the CS and CC calculations are carried out, and the number of K used in the CC calculation is up to 5.

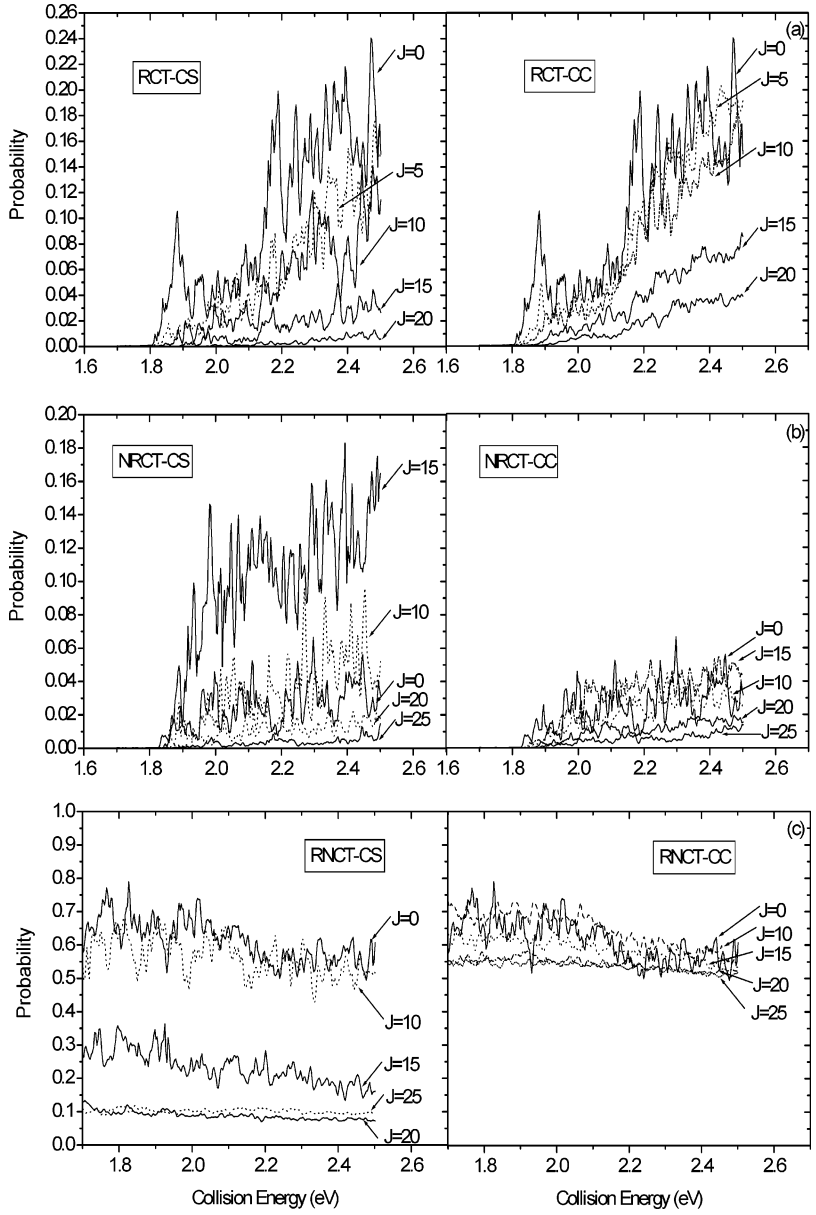

Figure 3. Calculated CS/CC probabilities as a function of collision energy in the energy range 1.7−2.5 eV: (a) for the RCT process $D^+ + H_2$ ($v = 0$, $j = 0$) → $DH^+ + H$ with $J = 0$, 5, 10, 15, and 20; (b) for the NRCT process $D^+ + H_2$ ($v = 0$, $j = 0$) → $D + H_2^+$ with $J = 0$, 10, 15, 20, and 25; (c) for the RNCT process $D^+ + H_2$ ($v = 0$, $j = 0$) → $H^+ + HD$ with $J = 0$, 10, 15, 20, and 25. Left panel, CS calculations; right panel, CC calculations.

Figure 3 shows the reaction probabilities obtained by the CS and CC calculations for the ground rovibrational initial state of H_2: (a) for $J = 0$, 5, 10, 15, and 20 for RCT, (b) for $J = 0$, 10, 15, 20, and 25 for NRCT, and (c) for $J = 0$, 10, 15, 20, and 25 for RNCT. Due to the deep well on the ground surface, many sharp, overlapping resonance peaks in the reaction probabilities appeared. As can be seen, both the RCT and NRCT results display an overall increasing trend with the increase of the collision energy, while the RNCT probabilities drop slightly as the collision energy is increased. At $J = 0$, a threshold energy of ∼1.8 eV was observed for both RCT and NRCT, and the "energy shift" at large J's caused by the centrifugal barrier was also observed in the two processes. Comparing the CS calculations with the corresponding exact calculations, it is apparent that the influence on the present system of neglecting the Coriolis coupling in the CS calculations is significant. The CS calculations produced much smaller reaction probabilities of the RCT and RNCT than the exact calculations. Besides, at high J, or at high collision energies for the same J, the CS values show much deviation from the CC results. For the NRCT, the CS influence is not only incarnated in the calculated values but also in the J-dependent behavior of the probabilities. As seen from Figure 3a and c, both the CS and CC probabilities of the RCT and RNCT decrease with increasing J nearly at each collision energy, whereas an abnormal J-dependent behavior of the CS probabilities is observed for the NRCT in that the probability tends to increase with increasing J for low J's of 0−15 and then decrease for higher J's. Nevertheless, such a feature has nearly disappeared in the CC calculations in that a significant decrease of the probability is found for the low J's of the same range, and also the deviation of the CS probability from the CC result tends to be small for higher J's, quite different from the RCT/RNCT.

A comparison of the present calculated probabilities for $J = 0$ of the RCT and NRCT channels with the time-independent results[11] is shown in Figure 4. One could find a reasonable agreement between both the calculated results in rich resonance structures and energy thresholds. However, quantitative differ-

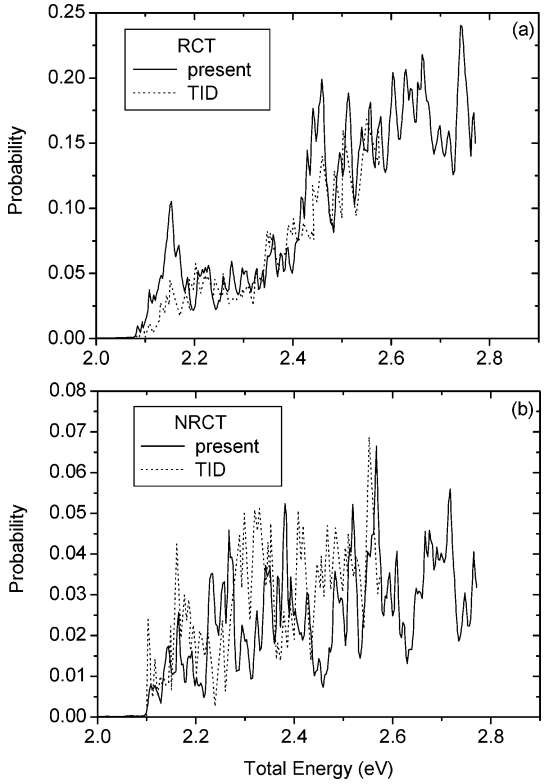

Figure 4. Comparison of probabilities for $J = 0$ between the previous time-independent and the present time-dependent quantum studies: (a) RCT; (b) NRCT.

ences, such as the peak positions and peak widths, are still found in the comparison, which, we believe, should be attributed to the different dynamical schemes. However, such differences have little effect on the calculated cross sections, since many of these resonance structures would be washed out through the total angular momentum J averaging (or J sum) in the calculations.

The quantum CS and CC cross sections for the ground rovibrational initial state of H_2 are shown in Figure 5: (a) for RCT, (b) for NRCT, and (c) for RNCT. In the calculated cross sections with the CS approximation, the resonance still survives and leads to the observed wiggling structures, whereas less wiggling structures are observed in the exact results due to the fact that more K states are included and therefore results in the further washing out of the resonance. It is also found that the CS approximation leads to the underestimation of the cross sections for the RCT/RNCT but the overestimation for the NRCT. In particular, it influences the RNCT most for which the largest deviation is observed between the CC and CS cross sections. Overall, there is an increasing trend in the cross sections of the RCT and NRCT and a decreasing trend in the RNCT over the whole investigated energy range. The cross sections of RCT and NRCT show noticeable thresholds of ~1.8 eV, similar to the probabilities of the two processes. In addition, the CC cross section also shows a nearly linear increase (decrease) as a function of collision energy for the RCT, NRCT (RNCT). A comparison between the present quantum results and the experimental measurements[41] is shown in Figure 6 for the RCT and RNCT processes only, because the experimental data for the NRCT channel are not available so far. There is an overall agreement of the general trend in cross sections over all collision energies considered. For the RCT process, the present quantum calculations give a threshold of ~1.8 eV, which is in good agreement with the experimental value 1.82 eV. Also,

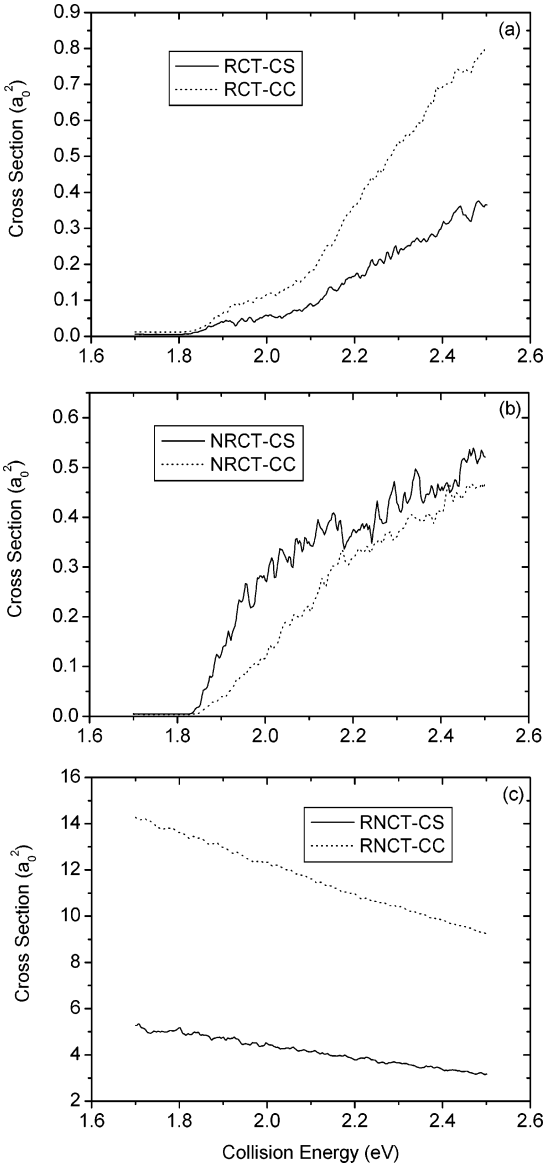

Figure 5. Calculated CS/CC total cross sections as a function of collision energy in the range 1.7−2.5 eV: (a) for the RCT process $D^+ + H_2$ ($v = 0$, $j = 0$) → $DH^+ + H$; (b) for the NRCT process $D^+ + H_2$ ($v = 0$, $j = 0$) → $D + H_2^+$; (c) for the RNCT process $D^+ + H_2$ ($v = 0$, $j = 0$) → $H^+ + HD$.

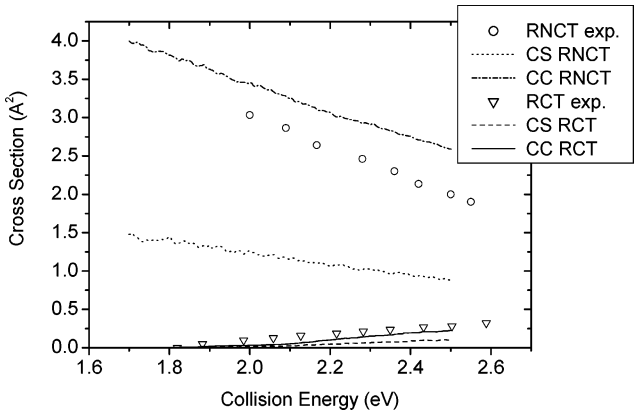

Figure 6. Comparison between the experimental data and the CS/CC calculated quantum cross sections.

the CC RCT cross sections agree reasonably well with the experimental results but the CS cross sections are somewhat

smaller. While, for the RNCT process, the computed CC quantum values are somewhat higher than the experimental results, we can see that a better improvement has been achieved with inclusion of the Coriolis coupling, since the corresponding CS cross sections are much lower than the experimental measurements. One of the most probable reasons for the discrepancy between our CC RNCT values and the experimental results is that the present calculations were carried out for the ground rovibrational initial state of the reactant H_2, whereas the experimental data were measured at room temperature.[41] Consequently, it is required that the exact quantum calculations on the rotational excited initial state $j = 1$ of the reactant H_2, which is the most probable j populated at room temperature, should be carried out in order to make the comparison more reasonable. However, such implementation needs further tedious effort that is quite beyond the scope of this work. In the meantime, we just performed the calculations on the $j = 1$ rotational initial state of H_2 for several J values, and the results showed that the H_2 rotational excitation mildly reduces the reaction probabilities. Thus, it is conceivable that better agreement can be reached between the experimental and the present CC RNCT cross sections if the exact calculations are carried out for the rotational excited initial state $j = 1$ for all possible J. It is worth noting that further experimental data are also required for carrying out a more quantitative comparison.

Figure 7 demonstrates the effect of the initial vibrational excitation on the reaction probabilities for $J = 0$. A remarkable increase in the RCT/NRCT probabilities is observed at a vibrational excitation of $v = 4$, indicating that the vibrational excitation of the reactant does enhance the nonadiabatic transition probabilities. Further, there is a slight preference to the NRCT enhancement of vibrational excitation, as compared with the RCT. Accordingly, the RNCT probability at $v = 4$ decreases to an average of 40−50%. It is also observed that at a collision energy of 2.1 eV the RCT probability exceeds the RNCT probability and that the sum of the RCT and NRCT probabilities is larger than the value of the RNCT for $v = 4$. These are due to the fact that $v = 4$ of H_2 is the most likely vibrational level to access the surface crossing seam.

A quantitative understanding of the reaction mechanisms can be obtained based on the present quantum results. It is demonstrated that, for the ground initial rovibrational state of reactant H_2, the RNCT dominates because it has the largest cross section of the three computed values. Since the RNCT occurs predominantly on the ground surface that favors an insertion mechanism due to the deep potential well, consequently, we can say, in other words, that the insertion mechanism has been shown to be the underlying mechanism for such reaction with H_2 in its ground initial state. Even though the formation of the nonadiabatic RCT/NRCT channels are always small in comparison with the RNCT channel at present, the different general trend as a function of energy exhibited by the three channels has, nonetheless, indicated the progressively opening up of the nonadiabtic channels for higher collision energy. This is quite understandable in that a high collision energy should provide more chance for the reactant to reach the crossing seams, a prerequisite for the occurrence of the nonadiabatic RCT and NRCT. Thus, at high collision energies, the nonadiabatic transition mechanism involving several potential energy surfaces may act and its contribution to the underlying mechanism increases slightly as the collision energy increases. Further, as shown in Figure 8, the alternative ascending fashion of the RCT/NRCT cross sections indicates that the two nonadiabatic channels are very competitive and comparable to each other at low collision energies, but once the collision energy exceeds 2.2 eV, the cross section of the RCT rises rapidly and becomes the favored channel. This can be explained as follows: With the prerequisite of being able to reach the crossing seams, the

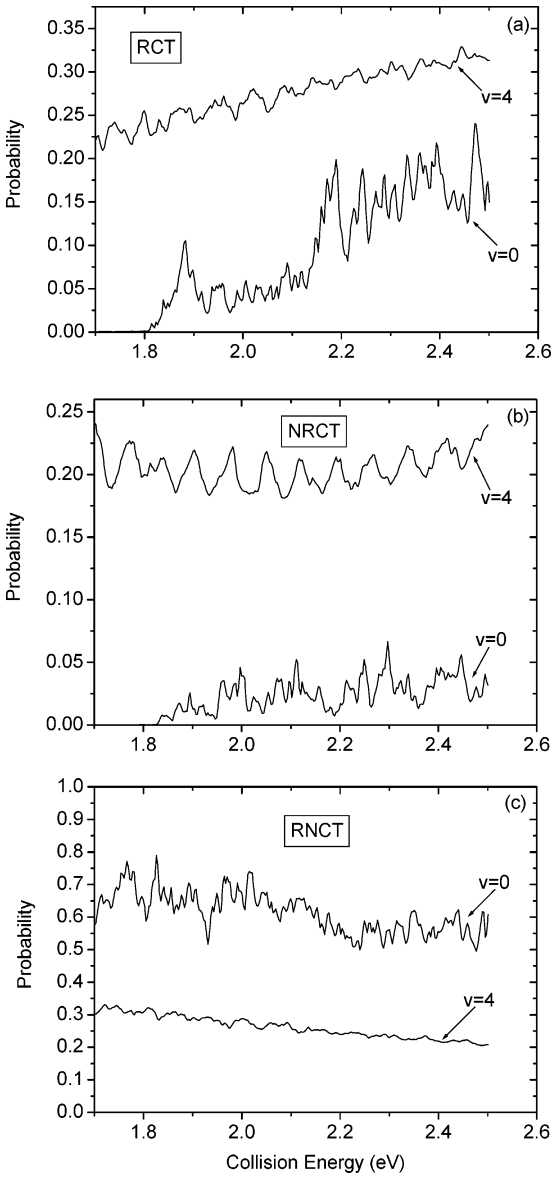

Figure 7. Calculated probabilities for $J = 0$ at the vibrational levels $v = 0$ and $v = 4$ of the reactant H_2 with $j = 0$, respectively: (a) RCT; (b) NRCT; (c) RNCT.

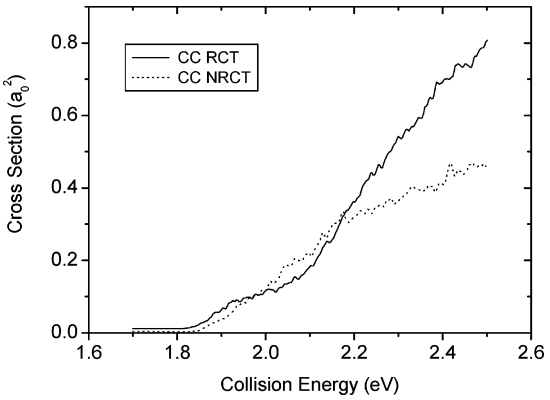

Figure 8. Computed CC cross sections for the two nonadiabatic processes of the RCT and NRCT.

reactant would then surmount the barriers on the excited surfaces to reach the product channels on the other side to form the RCT channel, or repel back to the reactant channels to open up the NRCT channel. For the reactant at collision energies below 2.2 eV, the opportunity of reaching the product side is almost the same as that of repelling backward, but at high collision energies, the former would overwhelm the latter, resulting in the slight preference for the RCT over the NRCT, although the two transition cross sections have magnitudes of the same order. Besides, the preference of the RCT may also arise from the contribution of the crossing seam located in the product channel, since the crossing seams of the system are known to be located both in entrance and exit asymptotic regions. In addition, the strong v dependence of the calculated probabilities revealed that the vibrational excitation of the reactant H_2, especially its closest level to the surface crossing of $v = 4$, plays a very important role in the electronically nonadiabatic transitions. The $v = 4$ results also suggest that, in the nonadiabatic transitions, the role of the vibrational excitation could be much more important than that of the translational excitation. Hence, it can be surmised that the RCT and NRCT should dominate over the RNCT when the reactant H_2 is excited to its vibrational level of $v = 4$ and that the nonadiabatic transition mechanism, instead of the insertion mechanism, contributes most to the reaction dynamics.

5. Conclusions

We have performed three-dimensional nonadiabatic quantum calculations for three competing processes of the RCT, NRCT, and RNCT in the $D^+ + H_2$ reaction system. In the calculations, the XSOS has been introduced to treat the multisurface problems. The main channel for the ground rovibrational initial state of the reactant H_2 is the RNCT, since it has the largest cross section. However, when H_2 is vibrationally excited, in particular to its closest level on the surface crossing, the nonadiabatic processes begin to dominate in the reaction system. Furthermore, a slight preference is found for the RCT at high collision energy in the two nonadiabatic processes that are of the same order of magnitude in cross sections. The comparison between the CS and CC calculations revealed that the CS approximation underestimates the cross sections of the RCT and RNCT but overestimates the cross section of the NRCT. Again, the poor agreement between the CS quantum values and the experimental data is attributed to the neglect of the Coriolis coupling in the CS approximation, and the exact CC quantum results reasonably agree with the experimental measurements. Our calculations demonstrated that inclusion of the Coriolis coupling is very important for an accurate calculation of the reactive system.

Acknowledgment. This work was supported by NKBRSF (1999075302), the Knowledge Innovation Program of Chinese Academy of Sciences (INF105-SCE-02-08), and NSFC (20373071, 20333050). The authors thank Professor Hiroki Nakamura for providing us the KBNN PES, and thanks are also to Mr. Xin Zhang for his valuable discussions.

References and Notes

(1) Tully, J. C.; Preston, R. K. *J. Chem. Phys.* **1971**, *55*, 562.
(2) Ochs, G.; Teloy, E. *J. Chem. Phys.* **1974**, *61*, 4930.
(3) Schlier, C.; Nowotny, U.; Teloy, E. *Chem. Phys.* **1987**, *111*, 351.
(4) Ichihara, A.; Shirai, T.; Yokoyama, K. *J. Chem. Phys.* **1996**, *105*, 1857.
(5) Billing, G. D.; Markovic, N. *Chem. Phys.* **1996**, *209*, 377.
(6) Markovic, N.; Billing, G. D. *Chem. Phys. Lett.* **1996**, *248*, 420.
(7) Markovic, N.; Billing, G. D. *Chem. Phys.* **1995**, *191*, 247.
(8) Last, I.; Gilibert, M.; Baer, M. *J. Chem. Phys.* **1997**, *107*, 1451.
(9) Ushakov, V. G.; Nobusada, K.; Osherov, V. I. *Phys. Chem. Chem. Phys.* **2001**, *3*, 63.
(10) Takayanagi, T.; Kurosaki, Y.; Ichihara, A. *J. Chem. Phys.* **2000**, *112*, 2615.
(11) Kamisaka, H.; Bian, W.; Nobusada, K.; Nakamura, H. *J. Chem. Phys.* **2002**, *116*, 654.
(12) Ichihara, A.; Yokoyama, K. *J. Chem. Phys.* **1995**, *103*, 2109.
(13) Viegas, L. P.; Cernei, M.; Alijah, A.; Varandas, A. J. C. *J. Chem. Phys.* **2004**, *120*, 253.
(14) Friedrich, O.; Alijah, A.; Xu, Z. R.; Varandas, A. J. C. *Phys. Rev. Lett.* **2001**, *86*, 1183.
(15) Tully, J. C. *J. Chem. Phys.* **1974**, *60*, 3042.
(16) Honvault, P.; Launay, J. M. *Chem. Phys. Lett.* **1999**, *303*, 657.
(17) Alexander, M. H.; Manolopoulos, D. E.; Werner, H. J. *J. Chem. Phys.* **2000**, *113*, 11084.
(18) Zhang, Y.; Xie, T. X.; Han, K. L. *J. Phys. Chem. A* **2003**, *107*, 10893.
(19) Schatz, G. C. *J. Phys. Chem.* **1995**, *99*, 7522.
(20) Schatz, G. C.; McCabe, P.; Connor, J. N. L. *Faraday Discuss. Chem. Soc.* **1998**, *110*, 139.
(21) Hoffmann, M. R.; Schatz, G. C. *J. Chem. Phys.* **2000**, *113*, 9456.
(22) Maiti, B.; Schatz, G. C. *J. Chem. Phys.* **2003**, *119*, 12360.
(23) Gray, S. K.; Goldfield, E. M.; Schatz, G. C.; Balint-Kurti, G. G. *Phys. Chem. Chem. Phys.* **1999**, *1*, 1141.
(24) Balint-Kurti, G. G.; Gonzalez, A. I.; Goldfield, E. M.; Gray, S. K. *Faraday Discuss.* **1998**, *110*, 169.
(25) Zhang, H.; Smith, S. C. *Phys. Chem. Chem. Phys.* **2004**, *6*, 4240.
(26) Zhang, H.; Smith, S. C. *J. Chem. Phys.* **2004**, *120*, 9583.
(27) Lin, S. Y.; Guo, H. *J. Chem. Phys.* **2004**, *121*, 1285.
(28) Lin, S. Y.; Guo, H. *J. Phys. Chem. A* **2004**, *108*, 2141.
(29) Xie, T. X.; Zhang, Y.; Zhao, M. Y.; Han, K. L. *Phys. Chem. Chem. Phys.* **2003**, *5*, 2034.
(30) Varandas, A. J. C.; Yu, H. G. *Chem. Phys. Lett.* **1996**, *259*, 336.
(31) Zhang, D. H.; Lee, S. Y. *J. Chem. Phys.* **1999**, *110*, 4435.
(32) Pack, R. T. *J. Chem. Phys.* **1974**, *60*, 633.
(33) McGuire, P.; Kouri, D. J. *J. Chem. Phys.* **1974**, *60*, 2488.
(34) Kosloff, R. *J. Phys. Chem.* **1988**, *92*, 2087.
(35) Zhang, D. H.; Zhang, J. Z. H. In *Dynamics of Molecules and Chemical Reactions*; Wyatt, R. E., Zhang, J. Z. H., Eds.; Marcel Dekker: New York, 1996; Chapter 6.
(36) Yang, B. H.; Tang, B. Y.; Yin, H. M.; Han, K. L.; Zhang, J. Z. H. *J. Chem. Phys.* **2000**, *113*, 7182.
(37) Zhang, X.; Yang, G. H.; Han, K. L.; Wang, M. L.; Zhang, J. Z. H. *J. Chem. Phys.* **2003**, *118*, 9266.
(38) Zhang, J. Z. H.; Dai, J.; Zhu, W. *J. Phys. Chem. A* **1997**, *101*, 2746.
(39) Alexander M. H.; DePristo, A. P. *J. Chem. Phys.* **1977**, *66*, 2166.
(40) Zhang, D. H.; Zhang, J. Z. H. *J. Chem. Phys.* **1993**, *99*, 6624.
(41) Schlier, Ch.; Nowotny, U.; Teloy, E. *Chem. Phys.* **1987**, *111*, 401.